Time-resolved studies of individual molecular rotors

2010 J. Phys.: Condens. Matter 22 264006

(http://iopscience.iop.org/0953-8984/22/26/264006)

J. Phys.: Condens. Matter **22** (2010) 264006 (11pp) doi:10.1088/0953-8984/22/26/264006

Time-resolved studies of individual molecular rotors

April D Jewell, Heather L Tierney, Ashleigh E Baber, Erin V Iski, Michael M Laha and E Charles H Sykes[1]

Department of Chemistry, Tufts University, 62 Talbot Avenue, Medford, MA 02155, USA

E-mail: charles.sykes@tufts.edu

Received 31 December 2009, in final form 10 March 2010
Published 14 June 2010
Online at stacks.iop.org/JPhysCM/22/264006

Abstract

Thioether molecular rotors show great promise as nanoscale models for exploring the fundamental limits of thermally and electrically driven molecular rotation. By using time-resolved measurements which increase the time resolution of the scanning tunneling microscope we were able to record the dynamics of individual thioether molecular rotors as a function of surface structure, rotor chemistry, thermal energy and electrical excitation. Our results demonstrate that the local surface structure can have a dramatic influence on the energy landscape that the molecular rotors experience. In terms of rotor structure, altering the length of the rotor's alkyl tails allowed the origin of the barrier to rotation to be more fully understood. Finally, time-resolved measurement of electrically excited rotation revealed that vibrational excitation of a C–H bond in the rotor's alkyl tail is an efficient channel with which to excite rotation, and that the excitation is a one-electron process.

(Some figures in this article are in colour only in the electronic version)

1. Introduction

Since its invention in 1981, the scanning tunneling microscope (STM) has been used to study myriad problems in surface chemistry, physics and nanoscience. The STM's atomic-scale resolution coupled with its ability to both track the motion of surface-bound molecules over time and position them accurately has opened many novel methods with which to study important nanoscale phenomena. One major limitation of STM imaging is the time resolution; conventional STMs record images over a period of a couple of minutes, giving a time resolution of ∼0.01 Hz. This is due to the limited bandwidth of the preamplifier that amplifies the tunneling current and enables the feedback loop to prevent the STM tip from crashing into the surface. The ability to image and record the progression of events on a surface in real time would provide unprecedented insight into the fundamental mechanisms of many important surface processes from nanoscience to catalysis. However, often the phenomena which interest surface scientists (i.e. diffusion, nucleation, reaction and surface reconstruction) occur on much faster timescales than conventional STM imaging can record [1].

Recent advances in fast-scanning STM technology, including the construction of very small STM heads using stiff materials with high resonant frequencies, have allowed for an increase in image acquisition rate up to ∼100 Hz [2–5]. A second option for tracking the dynamics of fast processes, pioneered by Don Eigler, involves lowering the sample temperature so that the processes being studied occur at a much lower rate. For example, a process that occurs at 10^{10} Hz at room temperature would take place less than once per minute if the system was cooled to 5 K. While low- and variable-temperature approaches have been very successful over the last 15 years, they are based on the assumption that molecular dynamics and surface structure are identical at the high and low temperatures.

Another option for increasing the time resolution of the STM involves direct measurement of the tunneling current with the feedback loop turned off. With this approach, changes in tunneling current can be correlated to conformational or positional changes of the molecule directly below (or in proximity to) the STM tip. The approach of measuring the tunneling current over time allows the dynamics of single molecules to be tracked with sub-nanometer precision and with a time resolution >1000 Hz. Researchers have used this approach to measure processes as fast as 20 000 Hz [6–25]. Our group has successfully exploited this measurement technique to study and characterize the dynamics of single-molecule rotors.

[1] Author to whom any correspondence should be addressed.

Our research in this field is aimed at uncovering the fundamental workings of surface-bound molecular rotors and investigating methods for directing their motion. In nature, molecular motors perform tasks such as powering the motion of individual cells (i.e. the bacterial flagellar motor), organizing the cellular cytoplasm by vesicle transport (i.e. kinesin or dynein), and even driving whole body locomotion via muscle contraction [26]. With the exception of liquid crystals, mankind has been unsuccessful in taking advantage of nanoscale molecular motion in designing and building devices. This is due in part to a gap in the understanding of how individual molecular components behave in the face of opposing forces such as friction, thermal fluctuations, coupling to neighbors and lack of inertia.

Organic chemists have been able to design and synthesize molecules in which rotation can be measured, turned on and off and even driven unidirectionally in solution using either photons or chemical power [27–29]. Very recently molecular rotors have even been used to measure microviscosity in living cells, a property linked to disease and malfunction [30–32]. However, much of the chemistry to date has focused on the synthesis of rotor molecules that, on paper, look similar to their macroscopic counterparts. This approach has provided many surprises: molecules with molecular structures that appear sterically restricted rotate freely, while others that look free have larger barriers to motion [33].

Understanding and actuating the rotation of individual molecules on surfaces is a crucial step towards the development of nanoscale devices such as fluid pumps, sensors, delay lines and microwave signaling applications [28]. Recent research in our group has employed low-temperature STM (LT-STM) experiments performed on a stable and robust system of thioether (RSR′) molecular rotors bound to metal surfaces [34, 35]. This system serves as a platform for characterizing the dynamics of individual molecular rotors as a function of temperature, rotor length, proximity of neighboring molecules and electrical excitation [6, 36–38].

2. Thioether molecular rotors

Recently a series of symmetric thioethers [$C_nH_{2n+1}SC_nH_{2n+1}$], with $n = 1, 2, 4$ and 6, were studied on a Au{111} surface [6]. In these simple systems, thioether (RSR′) molecules bind to the metal surfaces through a central S atom (the axle) and the alkyl tails (rotor) interact weakly with the surface, allowing the molecule to rotate if excited thermally. Scheme 1 shows a simple model of a static and a spinning dibutyl sulfide molecule (Bu_2S) [6, 36–38]. Au{111} was chosen as the first support for these molecules due to its inertness and binding strength to S-containing molecules. The investigation revealed that dimethyl sulfide (Me_2S) had a very low barrier to rotation (i.e. rotated at all accessible temperatures as low as 5 K), but the molecules with $n > 1$ had higher barriers. Unexpectedly, the larger molecules ($n = 2$, 4, and 6) all had roughly the same barrier to rotation. We initially hypothesized that the barrier to rotation was related to the interaction between the surface and the second (β) CH_2 group from the sulfur atom and that increasing the length of the alkyl tail would not significantly affect the torsional barrier [6].

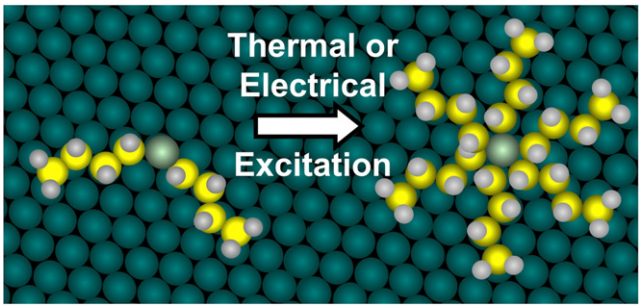

Scheme 1. Model of individual static and spinning dibutyl sulfide thioether molecular rotors.

The results of recent molecular dynamics (MD) simulations performed for several symmetric RSR molecules have demonstrated that the mechanism for rotation is more complex than our initial hypothesis suggested [38]. Calculations indicated that as the alkyl chain lengths increased, the van der Waals interactions with the metal surface increased, thereby driving the rotational barrier up. However, due to the flexibility of the alkyl tails, the number of atoms that strongly interact with the surface below did not change appreciably with an increased number of atoms. These two factors effectively cancel one another out; thus, the rotational barrier does not increase as the alkyl tails get longer in the range $n = 2$–6. As there is very little interaction of the alkyl tails of Me_2S with the surface, it is expected that this molecule would have a very low barrier to rotation as our experiments have shown [39]. In this paper we describe recent experimental work aimed at elucidating the factors that control the dynamics of both symmetric and asymmetric thioether molecular rotors. The two molecular rotors of interest are dibutyl sulfide (Bu_2S) and butyl methyl sulfide (BuSMe). In order to investigate the effect of surface composition and structure we have performed time-resolved dynamics experiments on both Au{111} and Cu{111} surfaces as shown in figure 1.

Au{111} has a unique structure commonly referred to as the *herringbone*, or technically, the $22 \times \sqrt{3}$ reconstruction [40–45]. The lower coordination of the Au surface atoms, as compared to the bulk, leads to a 4.4% contraction of the top layer with 23 gold atoms stacking along the $[1\bar{1}0]$ direction that would normally contain 22 atoms in the bulk. This results in the formation of domains of surface atoms with both hcp and fcc packing separated by soliton walls with an intermediate packing structure. The soliton walls appear as bright (red) lines in figure 1 that separate the hcp (narrow) and fcc (wide) domains. Cu{111} on the other hand is much simpler with flat {111} terraces, all of which are fcc in structure. While Au{111} is an ideal substrate for anchoring S-containing molecules, the heterogeneity in its surface structure means that measuring and understanding the dynamics of adsorbed species is a more complex task. This point will be discussed in detail later in the paper.

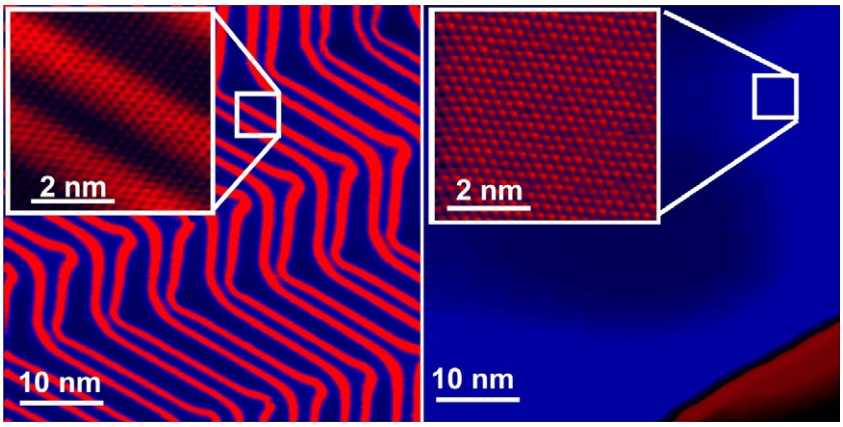

Figure 1. STM images of bare Au{111} (left) and Cu{111} (right) with insets showing atomic resolution. Imaging conditions: 78 K; Au: 50 pA, 500 mV (inset 900 pA, 50 mV); and Cu: 10 pA, −500 mV (inset 2 nA, 5 mV).

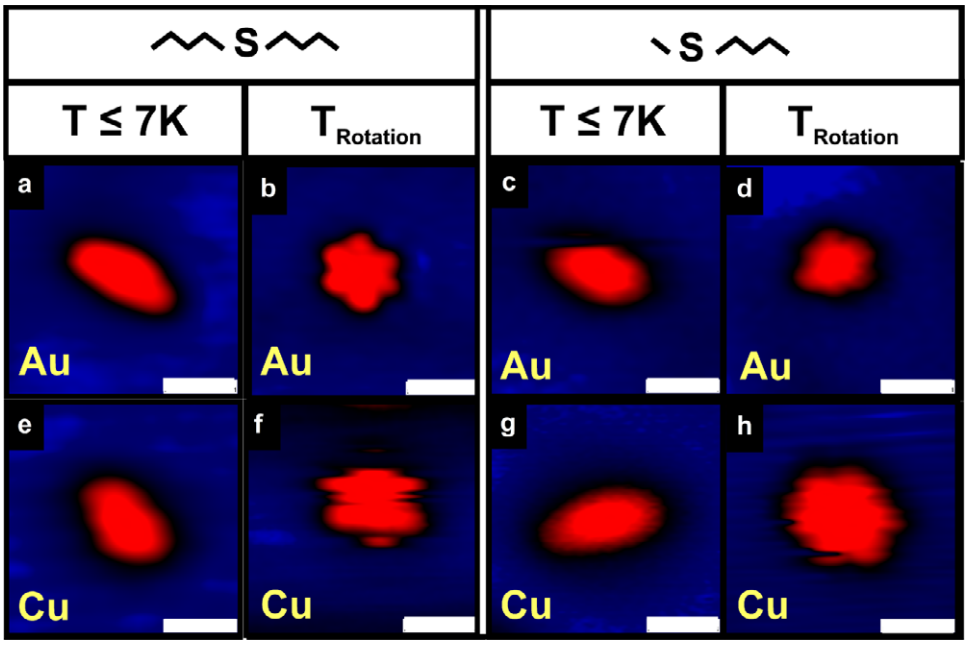

Figure 2. STM images showing thermal activation of dibutyl sulfide and butyl methyl sulfide molecular rotors on Au{111} (top row) and Cu{111} (bottom row) surfaces. Molecules (a), (c), (e) and (g) appear as roughly linear protrusions because they are stationary, while molecules (b), (d), (f) and (h) appear hexagonal in shape because they are rotating faster than the timescale of STM imaging. Scale bar = 1 nm. (Imaging conditions: 5–10 pA, ±50–300 mV (a) 7 K; (b) 35 K; (c) 7 K; (d) 22 K; (e) 7 K; (f) 9 K; (g) 5 K; (h) 8 K.)

3. Experimental details

All STM experiments described in this report were performed in a low-temperature, ultrahigh vacuum (LT–UHV) STM built by Omicron Nanotechnology [46]. The Au{111} and Cu{111} samples purchased from MaTeck were prepared under vacuum by cycles of Ar^+ sputtering (1.5 keV/10 μA) for 30 min followed by a 2 min anneal to 1000 K. This cycle was repeated approximately 12 times upon receiving the crystals. Between each STM experiment the crystals were prepared by 2 sputter/anneal cycles. After the final anneal, the crystals were transferred to the LT-UHV chamber ($< 5 \times 10^{-10}$ mbar) within 5 min to the pre-cooled STM stage. The sample cooled from room temperature to liquid N_2 or liquid He temperatures within approximately 1 h. All images were recorded with cut Pt/Ir or etched-W tips and voltages reported refer to the sample bias. Thioethers (between 99.9 and 99.95% purity) were obtained from Sigma Aldrich and were further purified by freeze/pump/thaw cycles prior to introduction to the STM chamber through a collimated molecular doser. The STM stage was equipped with a sample heater capable of controllably heating the sample and tip up to 50 K above the base temperature.

4. Results and discussion

Figure 2 shows STM images of individual thioether molecular rotors on both Au{111} and Cu{111} surfaces. The top

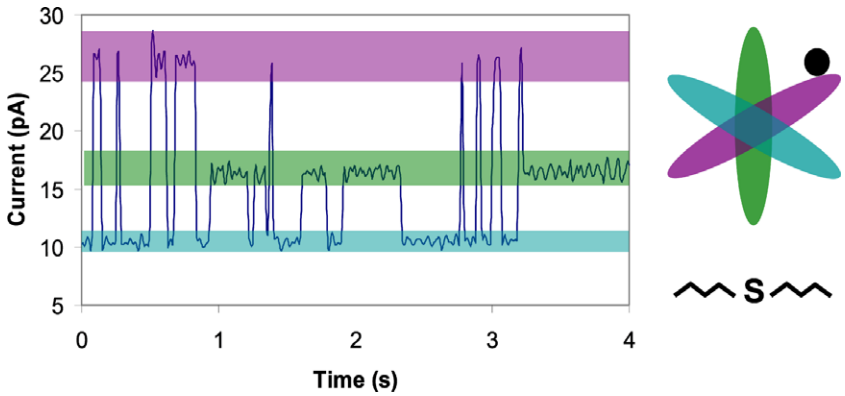

Figure 3. Tunneling current as a function of time (I versus t) curves for dibutyl sulfide on Cu{111} reveal three levels of tunneling current that correspond to the three inequivalent orientations of the molecule (purple, green and light blue) with respect to the STM tip position (black dot). Measurement conditions: 10 pA, 0.2 V, 11 K.

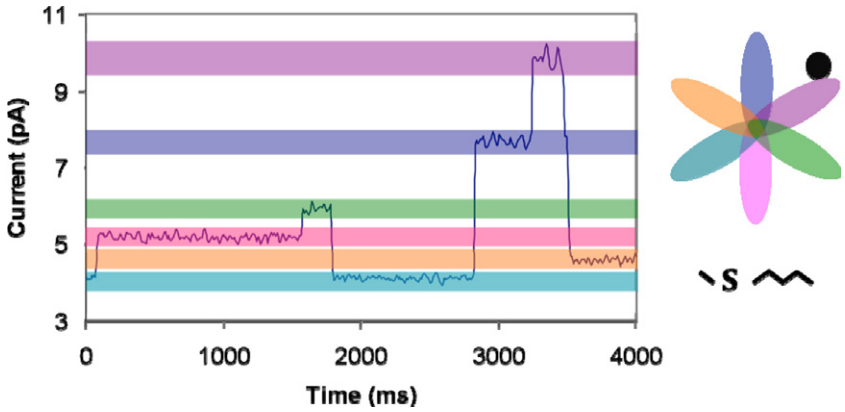

Figure 4. Tunneling current as a function of time (I versus t) plots for butyl methyl sulfide on Cu{111} reveal six levels of tunneling current that correspond to the six inequivalent orientations of the molecule's butyl tail (purple, blue, green, orange, pink and light blue) with respect to the STM tip (black dot). Measurement conditions: 5 pA, 0.2 V, 5 K.

row shows molecules on Au{111}, and the bottom row shows molecules on Cu{111}. The left block shows dibutyl sulfide (Bu_2S) molecules, and the right block shows butyl methyl sulfide (BuSMe) molecules. When imaging under nonperturbative scanning conditions and at temperatures $\leqslant$7 K, both molecules are static and appear in STM images as crescent-shaped protrusions as shown in the left column of each block of figure 2. The right column in each block of figure 2 shows images of molecular rotors at temperatures >7 K (see figure 2 caption for the temperature of each image). At elevated temperatures the molecules rotate via fast interconversion between six, equivalent orientations dictated by the high symmetry directions of the {111} surfaces. The molecular rotation occurs much faster than the timescale of STM imaging (ca. 2 min/image) thus; the molecules appear as hexagons due to the time averaged appearance of all six orientations [47, 48].

5. Time-resolved measurements

In order to characterize the rotation rates of single RSR′ molecules, tunneling current versus time (I versus t) experiments were performed. The feedback loop (which adjusts the STM tip–sample distance to maintain a constant tunneling current during imaging) was turned off during the I versus t measurements. As the thioether molecule rotated, the alkyl tails passed under the STM tip causing changes in the tunneling current. If the tip was placed just to the side of one of the six lobes of the hexagonal shape of the spinning molecule, as described previously for dibutyl sulfide, the tunneling current was observed to fluctuate between three discrete values [6]. We report here that the asymmetry of BuSMe leads to the appearance of six discrete values of the tunneling current during I versus t measurements (see figures 3 and 4 for a comparison of the molecules). These discrete tunneling current levels correspond to the three inequivalent orientations of Bu_2S (or six for BuSMe) with respect to the STM tip. The hexagonal arrangement of {111} surfaces imposes a hexagonal (or six-fold) symmetry on the preferred orientations of thioether molecular rotors [6, 36–38]. The three orientations of Bu_2S (as shown in figure 3) could be distinguished based on the different levels of tunneling current that arose depending on the position of the molecule with respect to the STM tip. The highest tunneling current corresponds to the orientation of the molecule one clockwise step (1-*cw*) from the tip (shown as a black dot); this orientation is shaded purple. The next

highest tunneling current corresponds to the 3-*cw* orientation (shaded in green) and the lowest current arises from the 2-*cw* orientation (shaded in light blue).

Since BuSMe is an asymmetric molecule, if the STM tip was carefully placed just to the side of one of the six lobes for I versus t spectroscopy measurements, the six states could be distinguished (as shown in figure 4). Assigning the tunneling current levels to specific molecular orientations is not as straightforward for BuSMe as it was for Bu_2S. To first approximation, as the tip is always positioned toward the edge of the molecule, the butyl tail contributes the majority of the tunneling current. Therefore, the highest tunneling current would correspond to the 1-*cw* molecular orientation (shaded purple), and successively lower tunneling currents correspond to the butyl tail located farther from the STM tip location (figure 4). In this simplified explanation, due to the asymmetry of the alkyl tails, the 4-*cw* lobe (light blue) directly across from the 1-*cw* lobe (purple) is no longer equivalent, and if the molecule rotated 180°, this would correspond to the lowest tunneling current. The remaining tunneling current levels are shaded according to the schematic in figure 4 (color online). In reality, the position of the methyl tail may have somewhat unpredictable contributions to the tunneling current. Therefore, the lowest tunneling current levels may not be assigned correctly due to a contribution from the methyl group. However, in terms of tracking the dynamics of motion, and in particular detecting directional motion, knowledge of the progression of a set of discrete levels is almost as valuable as an absolute assignment of the progression of orientation states. In simpler terms, directional motion would lead to a periodic, reproducible series of discrete current states, whereas random motion would yield a random progression.

It is interesting to note the relative magnitudes of the discrete tunneling current levels in figures 3 and 4. The separation of a particular current state and the state immediately below it decreases as the magnitude of the state decreases. Due to the exponential dependence of tunneling current on the tunneling gap width, as the molecule rotates away from the STM tip, the tunneling current will drop off in a pseudo-exponential fashion as is observed experimentally.

By using I versus t spectroscopy the rate and directionality of molecular rotations can be obtained on a timescale >1000 Hz. This allows for the characterization of molecular rotation with a resolution beyond what is achievable using STM imaging alone. Providing that one is consistent with the assignment of current levels to specific orientations of the molecule under investigation, it is possible to determine which way the molecule is rotating. In the case of Bu_2S, a current change or 'switch' from the high (1-*cw* or purple) current state to the low (2-*cw* or light blue) current state would signify a clockwise rotation, while a switch from the high (purple) current state to the intermediate (3-*cw* or green) current state would signify an anti-clockwise rotation. Using a similar approach, the rotations of the asymmetric molecule (BuSMe) can be characterized as clockwise or anti-clockwise. As discussed, the exact assignment of states is not necessary to monitor the progression through consecutive states with this technique as long as one is consistent with the assignments of current levels and molecular orientation.

In order to characterize the overall directionality of rotation, switches were labeled as positive (+) or negative (−), depending on the sequence of current levels. For example, a switch from orientation $a \rightarrow$ orientation b would be labeled as (+) and a $b \rightarrow a$ switch as (−). When the collection of switch assignments was examined for a particular data set, the degree to which rotation was unidirectional (i.e. more clockwise or anti-clockwise) would be indicated by the relative abundance of (+) and (−) switches. Approximately 13 000 thermally induced switches have been analyzed initially by hand for BuSMe on Cu{111} and the ± ratio was determined to be 49.8/50.2 (essentially 50/50). This ratio is expected as, according to the Second Law of Thermodynamics, it is not possible to get useful work from a system at thermal equilibrium [49]. Occasionally the change in tunneling current indicated a 180° rotation, making the ± assignment ambiguous. In these events the user would assign the rotation direction based on the sequence of current levels (e.g. low to high versus high to low) taking care to be consistent with any previous similar events. Analysis indicates that the predominant rotations are single 60° steps with 120° accounting for less than 35% and 180° less than 9% of rotations. Therefore, this approach can identify directionality associated with all but a few of the rotational events considered. While this presents a small problem in overall direction assignment, ultimately, any type of directional motion would lead to a periodic, reproducible series of discrete current states, whereas random motion would yield a random progression.

6. Automated switch counting

The I versus t curves generated with the feedback loop disabled often contained thousands of data points and hundreds to thousands of tunneling current changes, each representing a molecular reorientation, or 'switch'. For a graduate student collecting statistical data for many different molecules, counting these switches by hand would be a time consuming and daunting task. To that end, a computer program has been developed that quantifies the number of switches in each I versus t data set based on a set of user defined inputs for the tunneling current range of each molecular orientation (or 'state'). Each curve was initially examined by lab-personnel and a current range ('bin') for each state was defined and added to the program which then counted the number of switches within the curve. The program interrogated each point within the curve to determine if it fit within one of the defined bins, and if not the point was excluded from the data set. The program then compared consecutive points, ignoring excluded points; if consecutive points did not fall within the same bin, the computer recorded a switch. For example, if there were two bins defined as a and b, consecutive points (a–a–a) or (b–b–b) would not be counted as a switch, nor would points with the same bin assignment separated by an excluded point(s). However, (a–a–b) would be counted as one switch, and (a–b–a) would be counted as two switches.

The computer program also labeled each switch as positive (+) or negative (−) depending on the user defined sequence of orientational switches. Each I versus t curve was assessed

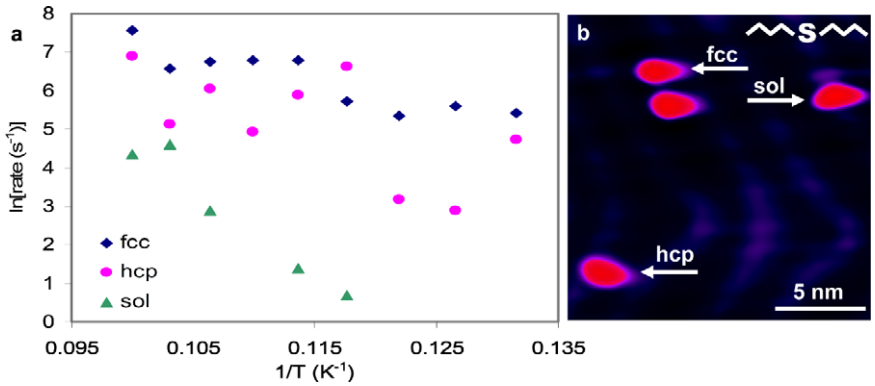

Figure 5. (a) Arrhenius plot for the rotation of individual dibutyl sulfide molecular rotors on the three different regions of the Au{111} $22 \times \sqrt{3}$ surface and (b) an STM image indicating the positions of three molecules interrogated. Rotation rates are obtained at each temperature from switching events in I versus t curves under nonperturbative measurement conditions (5 pA and 0.2 V). Imaging conditions: 5 pA, 0.2 V, 7 K.

and its output reported the total number of (+) and (−) switches which could be equated to rotations in opposite directions (i.e. clockwise or anti-clockwise). The program was used to characterize thermally induced rotation of BuSMe on Cu{111}, and the ratio of ± switches was determined to be 49.1/50.9 which indicates a slight preference for one direction. As mentioned, thermally driven rotation would always be expected to show no net directionality. The results from the automated analysis indicate a slight bias for rotation in one direction, which suggests that there may be a small error in the program itself. When I versus t curves from the same system were analyzed by hand the results indicated equal amounts of rotation in both directions. The bias in the automated analysis may indicate a limitation of the measurement itself, but it is likely that this represents an inherent limitation of the STM preamplifier's bandwidth and the computer's processing capabilities. Specifically, when rotational switching begins to occur faster than the response time of the tunneling current preamplifier, the I versus t curves no longer register a series of well-defined discrete tunneling currents connected by very steep changes in current. Instead, there is a lag time between discrete current states, and the computer program will erroneously identify switches that are not real. If the response times from higher to lower states and vice versa are different, then a non-existent state will be added to the curves in a regular fashion (i.e. $a - b - c$ instead of $a - c$) and lead to an apparent bias in one rotational direction. While this effect is always present when assigning the direction of rotation of individual molecular rotors, we have never observed an associated error larger than 6%. A lot of our future work will be aimed at coupling external sources of energy to more chemically complex rotors in order to induce highly directional rotation.

7. Arrhenius data

In order to investigate the energetic barriers for individual molecular rotors Arrhenius experiments were performed. The rates of rotation for individual rotors as a function of temperature were obtained by performing I versus t experiments at a variety of temperatures. Measurements were made for the rotation of Bu_2S molecules adsorbed on the fcc-regions, hcp-regions and the soliton walls of the Au{111} surface. Arrhenius plots for Bu_2S molecules in the three regions are shown in figure 5(a). The plots represent data taken for the molecules highlighted in figure 5(b). It is immediately evident from the graph that there is fair degree of scatter and a variability of the Arrhenius parameters for each molecule depending on where they reside. This is somewhat expected as the corrugation of the Au{111} surface gives rise to different electronic properties, and local strain within the surface itself that changes on a length scale of nanometers [40–45]. This leads to different binding properties for molecules depending on which part of the surface they are adsorbed [50–53]. From these Arrhenius measurements we found the average rotational barrier (E) of Bu_2S in the fcc-region was 1.2 ± 0.1 kJ mol^{-1} with an attempt frequency (A) of $7 \times 10^{7\pm0.3}$ Hz, while in the hcp-region $E = 0.8 \pm 0.1$ kJ mol^{-1} and $A = 1 \times 10^{6\pm0.5}$ Hz, and for a molecule adsorbed on the soliton wall $E = 2.0 \pm 0.8$ kJ mol^{-1} and $A = 1 \times 10^{12\pm4}$ Hz.

It is well known that the different regions of the Au{111} $22 \times \sqrt{3}$ surface gives rise to different electronic properties as well as different local structural properties (strain) within the surface itself, which changes on a length scale of nanometers. This has been shown to lead to different binding properties for molecules depending on which part of the surface they are adsorbed. It is however not usually possible to decouple the effect of strain from the electronic structure of the surface as both change in concert. While other studies have discussed adsorption effects in terms of electronics we do not believe that we can explicitly attribute the rotor energetics solely to surface strain or electronic effects.

These data reveal that the rotational energetics are strongly coupled with the molecule's exact position on the $22 \times \sqrt{3}$ surface reconstruction of Au{111}. In order to uncover the degree of variability arising from the Au reconstruction, Arrhenius data for several molecules in each area were recorded. Figure 6 shows Arrhenius plots for several individual molecules each adsorbed within one of the three regions (fcc, hcp and soliton wall) of the herringbone reconstruction. It

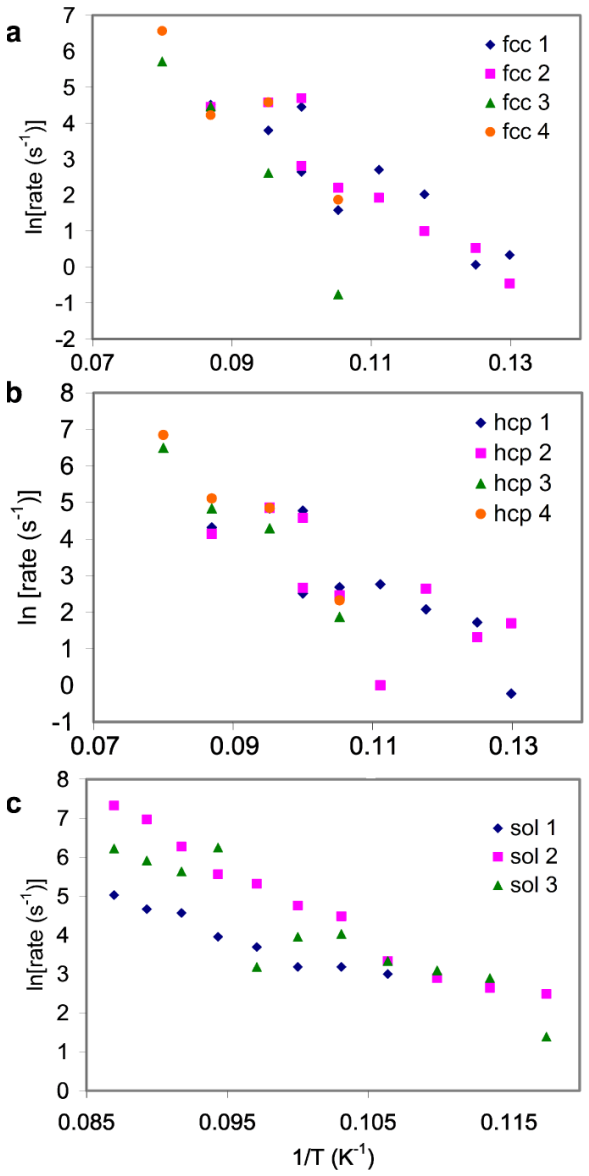

Figure 6. Arrhenius plots for several dibutyl sulfide molecules on the (a) fcc, (b) hcp and (c) soliton wall regions of Au{111} 22 × $\sqrt{3}$. All data was taken using nonperturbative measurement conditions (5 pA and 0.2 V).

can be seen from these plots that there is a great deal of variation, even for molecules within the same region of the surface. As the unit cell of the reconstruction is only 6.3 nm in width, moving a rotor laterally across the surface by only 0.1 nm changes the position of the molecule with respect to the different hcp, fcc and soliton regions significantly. As a result, the underlying surface properties change, as does the molecule's rotation rate. Therefore, it is expected that we observe such large variations within the Au{111} 22 × $\sqrt{3}$ data set. While much of the preliminary work for this study was performed using Au as a substrate, these results demonstrate that care must be taken in comparing the dynamics of molecular rotors on different areas of this surface.

In order to circumvent the variability introduced by the Au{111} surface structure itself, the rotational dynamics of Bu_2S molecules were also studied on a Cu{111} surface. The Cu{111} surface offers the same hexagonal symmetry as Au{111}, but without the complexity arising from the surface reconstruction (see figure 1). It is expected that a homogeneous surface structure would lead to less variability in the rotational dynamics data as, unlike on Au, the relative position of the rotor molecule in its equilibrium adsorption site on the Cu surface should not influence its barrier to rotation. Arrhenius data were obtained as before for several individual Bu_2S rotor molecules on Cu{111}. The plots are shown in figure 7(a) along with STM images (figure 7(b)) which indicate the molecules interrogated. The molecules in figure 7(b) are electrically excited at the imaging conditions used; thus they appear to spin. As expected, the data obtained for molecules on the Cu surface showed much less variability. These measurements yielded an average rotational barrier (E) of 1.48 ± 0.02 kJ mol^{-1} and an attempt frequency (A) of $8 \times 10^{7\pm0.8}$ Hz for Bu_2S on Cu{111}.

Our previous work on the rotation of thioether molecular rotors on Au{111} showed that dimethyl sulfide (Me_2S) has a very low barrier to rotation, while larger symmetric thioethers (diethyl, dibutyl and dihexyl sulfide) have roughly the same barrier (∼1.2 kJ mol^{-1}) [6, 39]. The results from the experiments reported herein suggest that Bu_2S has a slightly higher rotational barrier on Cu{111} than it does on Au{111}. This is an interesting result given that the phonon energy also differs between Cu and Au surfaces (Cu = 2.1 kJ mol^{-1}, $Au_{fcc,hcp}$ = 1.0 kJ mol^{-1} and Au_{sol} = 1.8 kJ mol^{-1}) [54]. One would naively expect that the energy of the surface phonons being excited during heating would directly map to the onset of excitation of molecular rotation. There is a weak correlation between the lower phonon energies of the hcp and fcc areas of Au and the higher phonon energies of Cu and the solution walls of Au and their respective torsional barriers (0.8 ± 0.1 kJ mol^{-1}, 1.2 ± 0.1 kJ mol^{-1}, 1.48 ± 0.02 kJ mol^{-1}, and 2.0 ± 0.8 kJ mol^{-1}). However, the fact that the correlation of torsional barrier with phonon energy is somewhat weak is not entirely unexpected given that the molecule–substrate interactions also change between Cu and Au. Our earlier molecular dynamics work also demonstrated that in addition to the rotor tail–substrate interaction, the S-metal bond strength also affects the rotational barrier [32]. Therefore, while this trend is obeyed qualitatively, phonon energies are not the only factor in determining molecular rotor energetics.

According to MD simulations, the rotational barrier for BuSMe should lie between that of Me_2S and Bu_2S [38]. An Arrhenius plot for several BuSMe molecules on Cu{111} is shown in figure 8(a), along with an STM image (figure 8(b)) indicating the molecules interrogated. The molecules in figure 8(b) appear to rotate due to effects arising from the relatively high voltage and current imaging conditions. Once again, the data show reasonably good reproducibility from molecule to molecule due to the homogeneity of the local Cu{111} surface structure. These measurements yielded an average activation barrier (E) of 740 ± 60 J mol^{-1} and an attempt frequency (A) of $2 \times 10^{7\pm0.4}$ Hz for BuSMe. The barrier to rotation for BuSMe on Cu{111} lies at an intermediate level between Me_2S and Bu_2S at ∼0.7 kJ mol^{-1}.

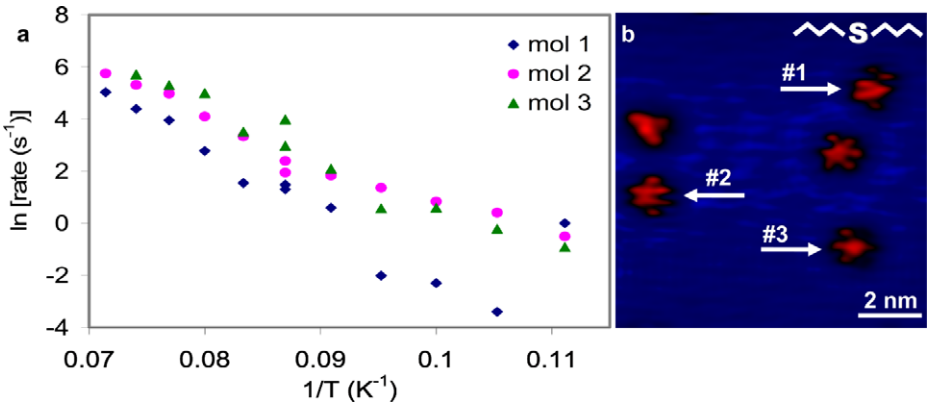

Figure 7. Arrhenius plots (a) for the rotation of three individual dibutyl sulfide molecules (mol 1, 2 and 3) on a Cu{111} surface. Rates of rotation for each temperature are obtained at nonperturbative tunneling conditions (10 pA and 0.2 V). (b) An STM image showing the molecules interrogated, the molecules appear to rotate because they are electrically excited at these imaging conditions: 100 pA, 0.2 V, 5 K.

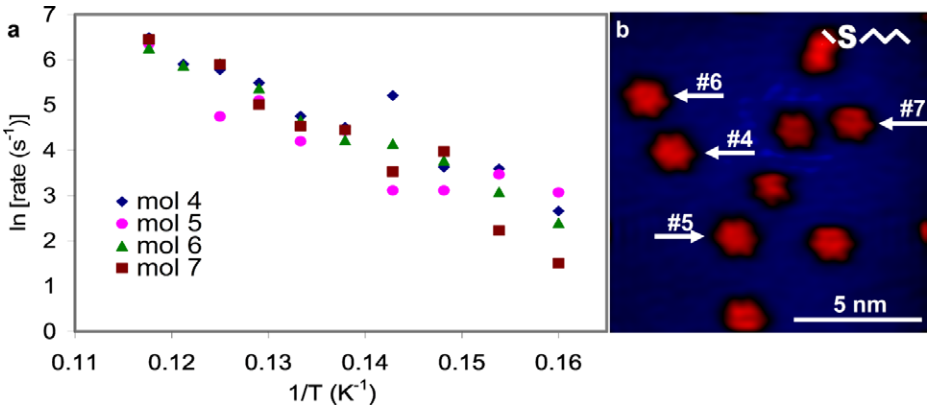

Figure 8. Arrhenius plots (a) for the rotation of four individual butyl methyl sulfide molecules (mol 4, 5, 6 and 7) on a Cu{111} surface. Rates of rotation are obtained for each temperature at nonperturbative tunneling conditions (10 pA and 0.2 V). (b) An STM image of the molecules interrogated; the molecules appear to rotate due to tip proximity effects at these imaging conditions: 400 pA, 0.5 V, 5 K.

This indicates that, to first approximation, the rotational barrier of thioether molecular rotors is a linear combination of each alkyl tail's barrier to rotation. Me_2S has a very low (unmeasurable) barrier, Bu_2S has a barrier $\sim$1.5 kJ mol^{-1}, therefore by this logic, BuSMe would be expected to have a rotational barrier of intermediate magnitude as is observed experimentally.

It is important to note that the attempt frequencies quoted for Bu_2S molecules on Cu{111} (figure 7) and on the fcc- and hcp-regions of Au{111} (figure 6) differ by several orders of magnitude from the expected range (10^{10}–10^{15} Hz) [55]. The value of A for BuSMe on Cu{111} is also unexpectedly low at $\sim 10^7$ Hz. Our initial hypothesis was that the Bu tails have many degrees of freedom, only a few of which have low rotational barriers. We investigated BuSMe with the expectation that its attempt frequency would be closer to the expected range, however, the results shown here indicate that even with one long tail removed, the rotors still have low attempt frequencies. Lyo and co-workers also recently reported a very low attempt frequency ($\sim 10^2$ Hz) for the chemisorption of ethylene on Si(001)c-(4 × 2); they attributed the low A value to entropic effects of the transition state [56]. This effect could be at play in our system if the rotor molecule becomes 'stiffer' as it transitions between its preferred rotational orientations. At this point further experiments on 'stiffer' molecules (PhSPh and rotors with conjugated/branched tails) are planned with the aim of understanding the low attempt frequencies observed experimentally.

For the Arrhenius plots presented in this paper, rates of rotation were obtained by counting the number of changes in tunneling current within the I versus t curves by hand and dividing the number of 'switches' by the total time in order to determine a rate of rotation at each temperature. An alternative method for determining a rate involves fitting the distribution of lifetime intervals of a particular state to an exponential and getting the rate directly from the inverse of the decay constant. This method has been employed to characterize a variety of systems with successful results but requires a lot more raw data in order to obtain reasonable exponential fits for each temperature [21, 22]. Our goal is to study the Arrhenius behavior of a wide variety of molecular rotors on different surfaces and to make relative comparisons of the systems. As such, we have found that good rate data can be obtained from counting raw numbers of events as described earlier and that smaller data sets can yield good fits.

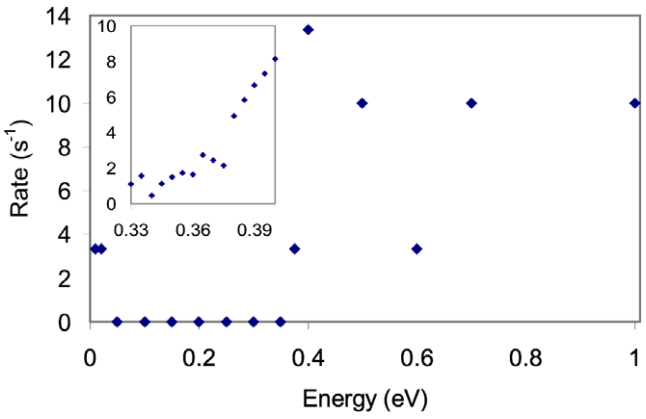

Figure 9. Action spectrum for a dibutyl sulfide rotor on the fcc-region of Au{111}. At electron energies approaching 0.4 eV a marked increase in rotation rate is observed. The inset shows higher resolution data from the 0.33–0.4 eV range that reveals that the onset of rotation occurs at an electron energy ∼375 meV, which correlates with a C–H stretch excitation. At very low voltages (<0.05 V) the tip–molecule distance is small, the barrier to rotation is lowered and a finite amount of rotation is observed. (Conditions: 5 pA and 7 K.)

8. Electrically inducing molecular rotation

The results discussed thus far demonstrate that relatively small amounts of thermal energy can induce the rotation of a variety of both symmetric and asymmetric thioether rotors. However, as previously stated, useful work cannot be derived from a purely isothermal process. In order to extract useful function from molecular rotors, methods for coupling them with external sources of energy to initiate rotation and eventually drive unidirectional rotation must be sought [16, 21, 22, 28, 49, 57–75]. Our experiments demonstrated that at temperatures below 8 K, larger ($n > 1$), symmetric RSR molecules were static and could be imaged stably for many hours at tunneling voltages less than ±0.35 V (nonperturbative conditions). However, either imaging or positioning the STM tip over the molecules at biases greater than ±0.35 V caused the molecules to rotate [6]. In order to elucidate the mechanism of this electrically excited rotation we performed Action Spectroscopy [16, 21, 22, 38, 57–63, 76]. This time-resolved technique correlates a molecular action (i.e. rotation) to the energy of electrons needed to induce the process. The action spectrum (a plot of rotation rates versus tunneling electron energy) for a Bu_2S molecule on the fcc-region of Au{111} is shown in figure 9. Such data characterizing the rotation of electrically excited Bu_2S molecules in different areas of the Au{111} surface showed marked increase in the rotational rate when tunneling electrons with energies above 375 ± 5 meV were injected into the molecule.

The energy onset was found to be independent of the direction of the tunneling electrons indicating an inelastic electron excitation of a molecular vibration. Furthermore, this onset energy range corresponds to a C–H stretching mode, which occurs at ∼360 meV [23, 77, 78]. Further experiments were performed using both Bu_2S and fully deuterated-Bu_2S (d-Bu_2S) on Au{111} and the action spectra showed a distinct

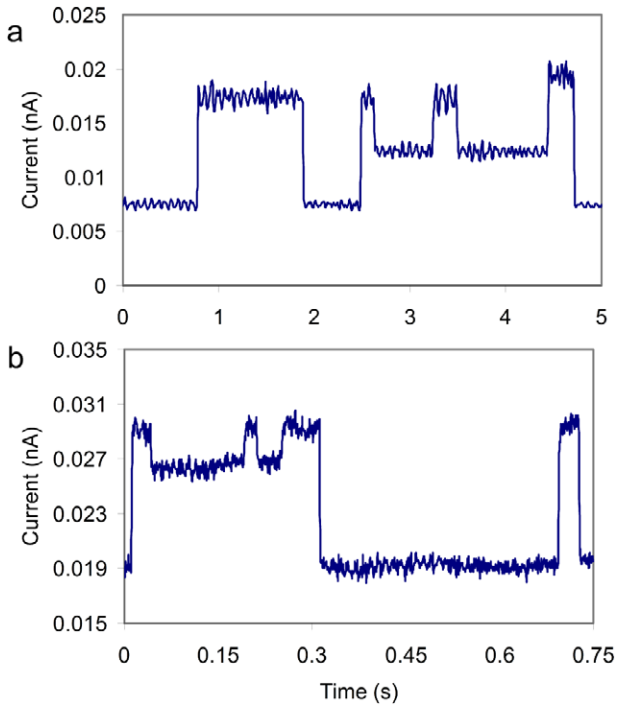

Figure 10. (a) Thermal versus (b) electrical I versus t curves for Bu_2S on Cu{111}. Thermal excitation populates all three rotational states equally whereas electrical excitation leads to shorter lifetimes of the orientations in which the molecule receives a higher flux of tunneling electrons. (Conditions: (a) 8.5 K, 0.2 V, 10 pA and (b) 7 K, 0.37 V, 10 pA.)

difference in the energy of the rotation onset [37]. For d-Bu_2S the onset energy shifted to 285 ± 5 meV, which is indicative of an isotope shift of $\sim 1/\sqrt{2}$ in the C–D stretch frequency [23, 77, 78]. These findings support the hypothesis that rotation of the molecule occurs via the excitation of a high-energy C–H or C–D stretch which then decays into different stretches, bends, and hindered rotations of the molecule and ultimately into rotation of the molecule as a whole. A finite amount of rotation was also observed at very low voltages (< ±0.05 V) as shown in figure 9. At these tunneling conditions the STM tip is very close to the molecule and can interact with it in a manner similar to the atomic manipulation mode [9]. We postulate that this low voltage effect arises not through any type of electronic excitation, but rather at close distances the tip forms a weak bond to the molecule, which decreases its interaction with the surface, thereby lowering its barrier to rotation.

9. Thermal versus electrical rotation

Figure 10 shows a representative plot of two I versus t curves for (a) thermally and (b) electrically induced rotation. These time-resolved plots illustrate that the lifetimes of the different rotational orientation states are effected by the mode of excitation. Visual inspection of the thermal plot reveals that the rotational orientations are all populated approximately equally. In the case of electrically excited rotation, the molecule spends more time in the states that correspond to

lower tunneling currents and considerably less time in the higher tunneling current states. When rotation is induced with thermal energy alone (i.e. with minimal perturbation by the STM tip), all rotational orientations with respect to the STM tip are populated to an equivalent degree. However, when rotation is induced with energetic electrons from the STM tip, the high current states (i.e states in which the rotor is closest to the tip and therefore receiving the highest flux of tunneling electrons) have the shortest lifetimes. This phenomenon arises because in the electrical excitation case, the electrons themselves are exciting the rotation of the molecule; the higher tunneling current orientations of the molecule receive a higher flux of electrons that excites rotation to other states. Therefore, the molecule exists in the high tunneling current states for the shortest period of time.

Each orientation state lifetime of the molecular rotors can be analyzed in order to deduce more about the mechanism of electrically excited rotation. In a tunneling electron induced process the rate of an event k is proportional to tunneling current I to the power n:

$$k \propto I^n.$$

The value of n indicates the number of electrons that are involved in the process. As the lifetime of a particular state τ is inversely proportional to the rate (k) of leaving the state:

$$\tau \propto \frac{1}{I^n}.$$

Therefore, high current states should have shorter lifetimes and low current states should have long lifetimes as is observed experimentally. Using the automated computer program the lifetimes of each state could be quantified and a rate of leaving each state calculated. Figure 11 shows a graph relating the rate of leaving each of the three states to the tunneling current the Bu_2S molecule receives in each state. On this *ln–ln* plot the gradient gives the n value and hence the order of the process. From inspection of figure 11 it appears that electrically driven rotation of Bu_2S on Cu{111} is a one-electron process. This result is consistent with a one-electron excitation of a C–H stretch at an energy of 375 meV that in turn leads to rotation of the whole molecule.

In summary, we have shown here the great utility of time-resolved measurements in obtaining quantifiable data on the dynamics and hence the energetics of molecular rotors on an individual molecule basis. I versus t curves allow many rotational events to be captured in a short time period. By correlating changes in the magnitude of the tunneling current to the position of the molecule with respect to the STM tip one can derive the direction of rotation of the rotor. The rate data from I versus t curves allows the effect of both thermal and electrical excitation to be studied in a quantitative manner. We find that surface structure and molecular chemistry have a great influence on the energetics of molecular rotation and that these effects can be used to uncover some of the fundamental mechanisms behind molecular rotation. Ultimately, in order for molecular rotors to do useful work they must be coupled to an external energy source. We show here that the STM tip

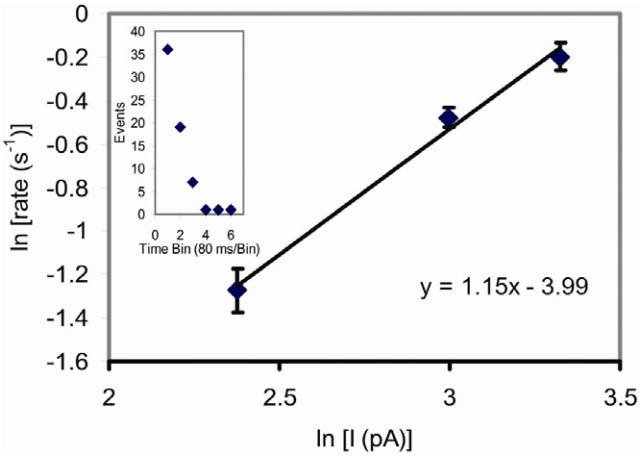

Figure 11. Plot of the rate of rotation of Bu_2S on Cu{111} as a function of tunneling electron current for electrically driven rotation with an electron energy of 370 meV. Inset shows a typical exponential lifetime distribution, in this case for the highest current state. The gradient of 1.15 indicates that electrical excitation occurs via a one-electron process. Conditions: 370 mV, 10 pA, and 7 K.

can act as a source of electrons that excite molecular rotation as well as monitor the rotation rate of the molecule being excited. These measurements reveal that molecular rotation can be driven electrically via excitation of a C–H stretch and that the electrical excitation is a one-electron process. Due to its relative ease of use and versatility this relatively new type of single-molecule time-resolved measurement will continue be a crucial tool in the quest to create nanoscale motors and devices.

Acknowledgments

The authors thank Research Corporation, NSF (Grant 0844343) and the Beckman Foundation for support of this research. ADJ thanks NSF for a graduate fellowship and HLT thanks the DOEd for a GAANN fellowship.

References

[1] Somorjai G A 1994 *Introduction to Surface Chemistry and Catalysis* (New York: Wiley)
[2] Besenbacher F, Lægsgaard E and Stensgaard I 2005 *Mater. Today* **8** 26–30
[3] Laegsgaard E, Osterlund L, Thostrup P, Rasmussen P B, Stensgaard I and Besenbacher F 2001 *Rev. Sci. Instrum.* **72** 3537–42
[4] Rost M J, Crama L, Schakel P, van Tol E, van Velzen-Williams G, Overgauw C F, ter Horst H, Dekker H, Okhuijsen B, Seynen M, Vijftigschild A, Han P, Katan A J, Schoots K, Schumm R, van Loo W, Oosterkamp T H and Frenken J W M 2005 *Rev. Sci. Instrum.* **76** 053710
[5] Wintterlin J, Trost J, Renisch S, Schuster R, Zambelli T and Ertl G 1997 *Surf. Sci.* **394** 159–69
[6] Baber A E, Tierney H L and Sykes E C H 2008 *ACS Nano* **2** 2385–91
[7] Gaudioso J and Ho W 2001 *Angew. Chem. Int. Edn* **40** 4080
[8] Gaudioso J, Lee H J and Ho W 1999 *J. Am. Chem. Soc.* **121** 8479–85
[9] Gimzewski J K and Joachim C 1999 *Science* **283** 1683–8

[10] Harikumar K R, Polanyi J C, Sloan P A, Ayissi S and Hofer W A 2006 *J. Am. Chem. Soc.* **128** 16791–7
[11] Hata K, Sainoo Y and Shigekawa H 2001 *Phys. Rev. Lett.* **86** 3084–7
[12] Krause S, Berbil-Bautista L, Herzog G, Bode M and Wiesendanger R 2007 *Science* **317** 1537–40
[13] Lauhon L J and Ho W 1999 *J. Chem. Phys.* **111** 5633–6
[14] Lozano M L and Tringides M C 1995 *Europhys. Lett.* **30** 537–42
[15] Moore A M, Mantooth B A, Donhauser Z J, Yao Y X, Tour J M and Weiss P S 2007 *J. Am. Chem. Soc.* **129** 10352
[16] Parschau M, Passerone D, Rieder K H, Hug H J and Ernst K H 2009 *Angew. Chem. Int. Edn* **48** 4065–8
[17] Ronci F, Colonna S, Thorpe S D, Cricenti A and Le Lay G 2005 *Phys. Rev. Lett.* **95** 156101
[18] Ronci F, Colonna S, Thorpe S D, Cricenti A and Le Lay G 2006 *Japan. J. Appl. Phys.* I **45** 2180–3
[19] Saedi A, Poelsema B and Zandvliet H J W 2009 *Phys. Rev.* B **79** 153402
[20] Saedi A, van Houselt A, van Gastel R, Poelsema B and Zandvliet H J W 2009 *Nano Lett.* **9** 1733–6
[21] Stipe B C, Rezaei M A and Ho W 1998 *Phys. Rev. Lett.* **81** 1263–6
[22] Stipe B C, Rezaei M A and Ho W 1998 *Science* **279** 1907–9
[23] Stipe B C, Rezaei M A and Ho W 1998 *Science* **280** 1732–5
[24] Wang K D, Zhang C, Loy M M T and Xiao X D 2005 *Phys. Rev. Lett.* **94** 036103
[25] Mugarza A, Shimizu T K, Ogletree D F and Salmeron M 2009 *Surf. Sci.* **603** 2030–6
[26] Schliwa M and Woehlke G 2003 *Nature* **422** 759–65
[27] Kay E R, Leigh D A and Zerbetto F 2007 *Angew. Chem. Int. Edn* **46** 72–191
[28] Kottas G S, Clarke L I, Horinek D and Michl J 2005 *Chem. Rev.* **105** 1281–376
[29] Michl J and Sykes E C H 2009 *ACS Nano* **3** 1042–8
[30] Haidekker M A, Brady T, Wen K, Okada C, Stevens H Y, Snell J M, Frangos J A and Theodorakis E A 2002 *Bioorg. Med. Chem.* **10** 3627–36
[31] Haidekker M A, Brady T P, Chalian S H, Akers W, Lichlyter D and Theodorakis E A 2004 *Bioorg. Chem.* **32** 274–89
[32] Haidekker M A and Theodorakis E A 2007 *Org. Biomol. Chem.* **5** 1669–78
[33] Schoevaars A M, Kruizinga W, Zijlstra R W J, Veldman N, Spek A L and Feringa B L 1997 *J. Org. Chem.* **62** 4943–8
[34] Jensen S C, Baber A E, Tierney H L and Sykes E C H 2007 *ACS Nano* **1** 423–8
[35] Jensen S C, Baber A E, Tierney H L and Sykes E C H 2007 *ACS Nano* **1** 22–9
[36] Bellisario D O, Baber A E, Tierney H L and Sykes E C H 2009 *J. Phys. Chem.* C **113** 5895–8
[37] Tierney H L, Baber A E, Jewell A D, Iski E V, Boucher M B and Sykes E C H 2009 *Chem.—Eur. J.* **15** 9678–80
[38] Tierney H L, Baber A E, Sykes E C H, Akimov A and Kolomeisky A B 2009 *J. Phys. Chem.* C **113** 10913–20
[39] Tierney H L, Calderon C E, Baber A E, Sykes E C H and Wang F 2010 *J. Phys. Chem.* C **114** 3152–5
[40] Barth J V, Brune H, Ertl G and Behm R J 1990 *Phys. Rev.* B **42** 9307–18
[41] Schaff O, Schmid A K, Bartelt N C, de la Figuera J and Hwang R Q 2001 *Mater. Sci. Eng.* A **319** 914–8
[42] Woll C, Chiang S, Wilson R J and Lippel P H 1989 *Phys. Rev.* B **39** 7988–91
[43] Voigtlander B, Meyer G and Amer N M 1991 *Phys. Rev.* B **44** 10354–7
[44] Huang K G, Gibbs D, Zehner D M, Sandy A R and Mochrie S G J 1990 *Phys. Rev. Lett.* **65** 3313–6
[45] Cho J W, Levy N, Kirakosian A, Comstock M J, Lauterwasser F, Frechet J M J and Crommie M F 2009 *J. Chem. Phys.* **131** 034707
[46] Becker T, Hovel H, Tschudy M and Reihl B 1998 *Appl. Phys.* A **66** S27–30
[47] Maksymovych P, Sorescu D C, Dougherty D and Yates J T 2005 *J. Phys. Chem.* B **109** 22463–8
[48] Rao B V, Kwon K Y, Liu A W and Bartels L 2004 *Proc. Natl Acad. Sci. USA* **101** 17920–3
[49] Astumian R D 1997 *Science* **276** 917–22
[50] Bohringer M, Morgenstern K, Schneider W D, Wuhn M, Woll C and Berndt R 2000 *Surf. Sci.* **444** 199–210
[51] Sykes E C H, Mantooth B A, Han P, Donhauser Z J and Weiss P S 2005 *J. Am. Chem. Soc.* **127** 7255–60
[52] Baber A E, Jensen S C and Sykes E C H 2007 *J. Am. Chem. Soc.* **129** 6368
[53] Gronbeck H, Curioni A and Andreoni W 2000 *J. Am. Chem. Soc.* **122** 3839–42
[54] Gawronski H, Mehlhorn M and Morgenstern K 2008 *Science* **319** 930–3
[55] Barth J V, Brune H, Fischer B, Weckesser J and Kern K 2000 *Phys. Rev. Lett.* **84** 1732–5
[56] Chung C H, Jung W J and Lyo I W 2006 *Phys. Rev. Lett.* **97** 116102
[57] Wahl M, Stohr M, Spillmann H, Jung T A and Gade L H 2007 *Chem. Commun.* 1349–51
[58] Komeda T, Kim Y, Kawai M, Persson B N J and Ueba H 2002 *Science* **295** 2055–8
[59] Ohara M, Kim Y, Yanagisawa S, Morikawa Y and Kawai M 2008 *Phys. Rev. Lett.* **100** 136104
[60] Pascual J I, Lorente N, Song Z, Conrad H and Rust H P 2003 *Nature* **423** 525–8
[61] Sainoo Y, Kim Y, Okawa T, Komeda T, Shigekawa H and Kawai M 2005 *Phys. Rev. Lett.* **95** 246102
[62] Wintjes N, Bonifazi D, Cheng F Y, Kiebele A, Stohr M, Jung T, Spillmann H and Diederich F 2007 *Angew. Chem. Int. Edn* **46** 4089–92
[63] Simic-Milosevic V, Meyer J and Morgenstern K 2009 *Angew. Chem. Int. Edn* **48** 4061–4
[64] Chiaravalloti F, Gross L, Rieder K H, Stojkovic S M, Gourdon A, Joachim C and Moresco F 2007 *Nat. Mater.* **6** 30–3
[65] Vaughan O P H, Williams F J, Bampos N and Lambert R M 2006 *Angew. Chem. Int. Edn* **45** 3779–81
[66] Stöhr M, Wagner T, Gabriel M, Weyers B and Möller R 2001 *Phys. Rev.* B **65** 033404
[67] Astumian R D and Hanggi P 2002 *Phys. Today* **55** 33–9
[68] Ohara M, Kim Y and Kawai M 2008 *Phys. Rev.* B **78** 201405
[69] Komeda T, Kim Y, Fujita Y, Sainoo Y and Kawai M 2004 *J. Chem. Phys.* **120** 5347–52
[70] Vacek J and Michl J 2007 *Adv. Funct. Mater.* **17** 730–9
[71] Wang B Y, Vukovic L and Kral P 2008 *Phys. Rev. Lett.* **101** 186808
[72] Zhong D, Blömker T, Wedeking K, Chi L, Erker G and Fuchs H 2009 *Nano Lett.* **9** 4387–91
[73] Joachim C and Gimzewski J K 2001 *Molecular Machines and Motors* (Berlin: Springer) pp 1–18
[74] Gao L, Liu Q, Zhang Y Y, Jiang N, Zhang H G, Cheng Z H, Qiu W F, Du S X, Liu Y Q, Hofer W A and Gao H J 2008 *Phys. Rev. Lett.* **101** 197209
[75] Gimzewski J K, Joachim C, Schlittler R R, Langlais V, Tang H and Johannsen I 1998 *Science* **281** 531–3
[76] Kawai M, Komeda T, Kim Y, Sainoo Y and Katano S 2004 *Phil. Trans. R. Soc.* A **362** 1163–71
[77] Lauhon L J and Ho W 2000 *Phys. Rev. Lett.* **84** 1527–30
[78] Sainoo Y, Kim Y, Komeda T and Kawai M 2004 *J. Chem. Phys.* **120** 7249–51